

Isospin asymmetry and neutron stars in V-QCD

Lorenzo Bartolini¹, Sven Bjarke Gudnason¹, Matti Järvinen^{2,3}

¹*Institute of Contemporary Mathematics, School of Mathematics and Statistics, Henan University, Kaifeng, Henan 475004, P. R. China*

²*Asia Pacific Center for Theoretical Physics, Pohang 37673, Republic of Korea*

³*Department of Physics, Pohang University of Science and Technology, Pohang 37673, Republic of Korea*

E-mail: [lorenzo\(at\)henu.edu.cn](mailto:lorenzo@henu.edu.cn), [gudnason\(at\)henu.edu.cn](mailto:gudnason@henu.edu.cn),
[matti.jarvinen\(at\)apctp.org](mailto:matti.jarvinen@apctp.org)

ABSTRACT: Isospin asymmetric nuclear matter is introduced to V-QCD, a bottom-up holographic Quantum Chromodynamics (QCD) model. Using a small isospin chemical potential we extract the symmetry energy in the model, finding excellent agreement with experimental results for some of the potentials. Extending the calculation for finite and arbitrary sized isospin chemical potentials, we construct β -equilibrated neutron stars via the usual Tolman-Oppenheimer-Volkov (TOV) equations. We find, pleasingly, that the neutron stars passing the mass/radius and tidal deformability constraints are those with the potentials that also lead to excellent symmetry energies.

KEYWORDS: Holographic QCD, V-QCD, isospin asymmetry, neutron stars

Contents

1	Introduction	1
2	The model	4
3	Symmetric nuclear matter	8
4	Isospin asymmetry	9
4.1	Small isospin approximation: Symmetry energy	10
4.2	General configuration: β -equilibrated neutral matter	14
5	Quark phase	16
6	Neutron stars	18
7	Conclusions	21
A	Vanishing contribution of variation of r_c to the symmetry energy	23
B	Tables of parameters	24

1 Introduction

Quantum Chromodynamics is the established fundamental theory of the strong nuclear interactions. Due to asymptotic freedom, a property of non-Abelian quantum gauge theories with sufficiently little matter content, QCD is weakly coupled at high energies, where perturbative QCD (pQCD) becomes reliable. Unfortunately, the low-energy world of nuclei – protons and neutrons – is then described by QCD at strong coupling. Lattice formulation of QCD (LQCD) is a powerful numerical tool that can calculate observables on a discretized Euclidean space (a four-dimensional hypercube). Unfortunately, due to a technical problem called the sign problem [1], LQCD struggles to converge when chemical potentials are introduced, which is needed for simulating QCD at finite densities. Neutron stars are beautifully the most compact objects in the Universe that have not collapsed into black holes and they provide us with data on mass, radius, and spin etc. – but they are at the nexus of the above-described problems: Low energies and large densities.

The AdS/CFT correspondence is a powerful tool as a mathematical duality: It maps couplings, numbers and observables on one side of the duality to the other side. The

fascinating property of this duality in particular, is that it also maps strong coupling to weak coupling: A strong coupled field theory on the boundary of a d -dimensional AdS spacetime is mapped to a weakly coupled gravitational theory in the bulk of said $d + 1$ dimensional AdS. The main and strongest evidence for this duality was found by Maldacena in his seminal 1997 paper [2], mapping the entire spectrum of primary operators of the superconformal field theory, i.e. $\mathcal{N} = 4$ super-Yang-Mills (sYM), to AdS in five dimensions with independence from coordinates on a 5-sphere. Superconformal field theories or simply conformal field theories (CFTs) have limited usage for particle physics, with the exception of some ideas denoted unparticle physics [3], since they describe field theories without reference to any scale or any size. Hence, they are not suitable for particle physics, such as QCD.

Unlike the case of $\mathcal{N} = 4$ sYM theory, holographic models for strong interactions, dubbed holographic QCD (HQCD), have not been derived with strong evidence for the duality to hold true and it would often be better to say they are holographic models, than dual theories to true QCD. Nevertheless, they are born with a strong-weak duality built-in and are usually constructed to assimilate the properties of strong interactions or at least main aspects thereof.

Generally speaking, there are two kinds of holographic QCD models: Top-down models that are based on string theory constructions, such as the D3/D7 model [4], Witten-Sakai-Sugimoto model [5, 6], etc. They have the advantage of having a full-fledged string theory in the UV, which builds in some consistency in the models, although the UV theory is usually a web of D-branes and most likely not exactly the CFT that QCD flows to at large (infinite) energies. Another branch of HQCD models are called bottom-up as they are engineered to describe QCD purely from phenomenological considerations or even (L)QCD data. Popular models studied in recent years fall in the classes of hard-wall [7] or soft-wall models [8].

In this paper, we will work with V-QCD [9–20] which is a bottom-up HQCD model that is inspired by the Veneziano limit, which is a variation of the 't Hooft large- N_c limit. More precisely, the 't Hooft large- N_c limit of gauge theories corresponds to a fixed number of flavors with the number of colors, N_c being sent to infinity [21]. Rescaling the gauge coupling $g_{\text{YM}}^2 \rightarrow g_{\text{YM}}^2/N_c$, observables remain finite with $1/N_c$ corrections in the large- N_c limit. The Veneziano limit [22] on the other hand, also sends the number of flavors to infinity as:

$$N_f \rightarrow \infty, \quad N_c \rightarrow \infty, \quad x_f \equiv \frac{N_f}{N_c} \text{ fixed}, \quad (1.1)$$

and imposing the same scaling for the gauge coupling as in the 't Hooft limit. The “V” in the name of the model refers to the fact that the string theory inspiration of the model makes use of this limit. The V-QCD model is, however, a bottom-up model with gluon and quark degrees of freedom, where the quarks are fully backreacted to the glue background, which corresponds formally to the Veneziano limit given above. The V-QCD model parameters are determined by comparing observables to (L)QCD data at finite (and small) values of N_c and N_f in the end. See ref. [23] for a recent review of the model.

Neutron stars have been considered previously in HQCD models, in particular in WSS with isospin asymmetry [24–26], in D3/D7 without isospin asymmetry [27–29], in hard-wall without isospin asymmetry [30], in V-QCD without isospin asymmetry [31–35], and in V-QCD using a hybrid setup where the isospin dependence was borrowed from a field theory model [36–38]¹: Isospin symmetric matter is the case where protons and neutrons are considered on equal footing as a rough approximation. Neutron stars are, however, made up of mostly neutrons as the large density allows for the baryons to be unstable (i.e. to be neutrons) because they are neutral and hence do not suffer from Coulomb repulsion. In order to take this properly into account in HQCD, isospin asymmetry must be incorporated. Although isospin asymmetric baryonic matter has been considered previously in HQCD [40–42, 26] as well as for neutron stars in the WSS model [24–26], it has not been ported to V-QCD, where the fits to LQCD infuses real-world QCD phenomenology into the model, until now.

In order to consider an object as large as a neutron star with such a large density in its interior, it is often approximated as a homogeneous matter of neutrons and protons inside, where there is no tracing of where there protons or neutrons are, but simply how many there are per unit volume.² This can be approximated by the so-called homogeneous Ansatz for baryonic matter in HQCD [50] together with a chemical isospin potential, which is imposed on the boundary, according to the holographic dictionary. Apart from drastically simplifying the analysis, the use of this Ansatz circumvents phenomenological issues such as the fact that the holographic large- N_c dense nuclear matter phase is a crystal [51, 52], rather than a superconducting liquid.

In this paper, we port for the first time isospin asymmetric baryonic matter to the precision fit-to-LQCD V-QCD holographic model of QCD, calculate the symmetry energy as well as fully nonlinearly backreacted asymmetric baryonic matter with finite isospin for the computation of nonspinning neutron stars. Using the TOV equations we compute the corresponding mass-radius curves for neutron stars and further compute the β -equilibrated neutral neutron/proton/electron/muon composition of the stars.

V-QCD has already been established as precision holographic model for quite some time. A recent and necessary development in the model was the advancement of determining the Chern-Simons (CS) term [53]. Although not important for the pure glue sector, the CS term is of utter importance for the baryon [54], since the stabilization of the size and position in the holographic direction depends strongly on the CS. This work on the CS is thus a necessary step as it determined the functional form and coefficients of some of the functions entering the CS term. We will, however, take a few of the parameters as free parameters in this work, see below.

We find, albeit a rescaling is necessary for compensating some of all the approximations done in the process of building this model, that the symmetry energy is surprisingly better

¹A study of neutron star matter in an Einstein-Maxwell-dilaton-scalar theory includes isospin asymmetry, but fixes the proton fraction by hand [39]

²Neutron stars have also been studied in the Skyrme model, both in the homogeneous approximation [43–47] as well as with baryonic crystals [48, 49].

than in the WSS model [41] and the neutron stars for some of the potentials can pass all the phenomenological mass/radius/tidal deformability bounds. More interestingly, we find that the equations of state that give rise to good symmetry energies *also* lead to neutron stars well inside the experimental constraints.

The paper is organized as follows. In sec. 2 we introduce the model and set our notation. In sec. 3 the homogeneous Ansatz and symmetric matter is reviewed. In sec. 4, isospin asymmetric matter is introduced into V-QCD following a generalized Ansatz previously used in the WSS and the symmetry energy is presented. In sec. 5, the possibility of a pure quark phase is considered. In sec. 6, we finally present our results on the neutron stars. We conclude with a discussion in sec. 7. Some details are delegated to appendices A and B.

2 The model

We consider V-QCD which is a holographic bottom-up model dual to QCD with both gluon and quark degrees of freedom and full backreaction of the quarks to the glue [13]. The V-QCD model is built around two main sectors, the glue and the flavor: The glue sector is described by Improved Holographic QCD (IHQCD) [9, 10], a bottom-up model for Yang-Mills theory inspired by five-dimensional noncritical string theory. The flavor sector is described by Tachyonic Dirac-Born-Infeld (TDBI) and Tachyonic Chern-Simons (TCS) actions arising from a pair of space-filling D4 branes [55, 56].

The holographic dictionary between the five-dimensional fields in gravity and their dual operators in QCD is the following:

- The metric g_{MN} is dual to the energy-momentum tensor $T_{\mu\nu}$, where Latin (Greek) indices are five (four) dimensional.
- The dilaton ϕ is dual to the $G_{\mu\nu}^a G^{\mu\nu a}$ operator, where $G_{\mu\nu}^a$ is the field strength of the gluons and a is the adjoint color index.
- The tachyon T^{ij} , a complex matrix field with the flavor indices $i, j = 1 \dots N_f$, is dual to the quark bilinear operator $\bar{\psi}^i \psi^j$.
- The left- and right-handed gauge fields $(A_M^{L/R})^{ij}$ are dual to the left- and right-handed current operators $\bar{\psi}^i (1 \pm \gamma_5) \gamma_\mu \psi^j$.

Note that here the first two fields are related to the gluonic degrees of freedom. They arise from the closed string degrees of freedom in string theory. The latter two fields are flavor fields, coming from the space-filling branes, and describe open string degrees of freedom.

The action for IHQCD consists of two terms,

$$S_{\text{IHQCD}} = S_g + S_{\text{GH}}, \quad (2.1)$$

where the first term is the five-dimensional Einstein-dilaton gravity action and the second term is the Gibbons-Hawking boundary term:

$$S_g = M_p^3 N_c^2 \int d^5x \sqrt{-\det g} \left[R - \frac{4}{3} g^{MN} \partial_M \phi \partial_N \phi + V_g(\phi) \right], \quad (2.2)$$

$$S_{\text{GH}} = M_p^3 N_c^2 \int d^5x \sqrt{-\det h} K. \quad (2.3)$$

Here M_p is the five-dimensional Planck mass, V_g is the dilaton potential, and h is the pull-back of the five-dimensional metric g on the four-dimensional boundary, while R, K are respectively the scalar and extrinsic curvature. The five-dimensional metric g is calculated using the Ansatz

$$ds^2 = e^{2A(r)} \left(\frac{dr^2}{f(r)} - f(r) dt^2 + d\vec{x}^2 \right). \quad (2.4)$$

We choose the UV boundary to be at $r = 0$, while for the IR behavior there are different choices, determined by of the blackening factor $f(r)$. In this work, we will be interested in nuclear matter in the zero temperature confined phase, hence we will set $f(r) := 1$.

The TDBI action is given by

$$S_{\text{TDBI}} = -\frac{1}{2} M_p^3 N_c \text{tr} \int d^5x \left(V_f(\phi, T^\dagger T) \sqrt{-\det \mathbf{A}_L} + V_f(\phi, TT^\dagger) \sqrt{-\det \mathbf{A}_R} \right), \quad (2.5)$$

with tr denoting the trace over the flavor indices and

$$\begin{aligned} \mathbf{A}_{L,MN} &= g_{MN} + w(\phi, T^\dagger T) F_{MN}^{(L)} + \frac{\kappa(\phi, T^\dagger T)}{2} \left[(D_M T)^\dagger (D_N T) + (D_N T)^\dagger (D_M T) \right], \\ \mathbf{A}_{R,MN} &= g_{MN} + w(\phi, TT^\dagger) F_{MN}^{(R)} + \frac{\kappa(\phi, TT^\dagger)}{2} \left[(D_M T) (D_N T)^\dagger + (D_N T) (D_M T)^\dagger \right], \\ D_M T &= \partial_M T + iT A_M^L - iA_M^R T, \\ F_{MN}^{(L/R)} &= \partial_M A_N^{L/R} - \partial_N A_M^{L/R} - i[A_M^{L/R}, A_N^{L/R}], \end{aligned} \quad (2.6)$$

where $\mathbf{A}_{L/R}$ are matrices in the square root of the TDBI action, not to be confused with $A_M^{L/R}$ which are gauge fields.

We will consider simple choices for the tachyon and dilaton dependence of the various potentials following refs. [13, 31]: In particular, we will assume the tachyon to be proportional to the unit matrix $T = \tau(r)\mathbf{1}$, as appropriate for a setup with identical quark masses (we will work with vanishing quark masses), and an exponential potential in the squared tachyon for the function V_f :

$$V_f(\phi, TT^\dagger) = V_{f0}(\phi) e^{-\tau^2}, \quad (2.7)$$

and assume tachyon dependence to be absent for other functions: $\kappa = \kappa(\phi)$, $w = w(\phi)$.

We follow the usual approach with nuclear matter in gauge/gravity duality, and treat the gauge fields in the action as probe fields. That is, we replace eq. (2.5) by its leading

order expansion in the terms involving gauge fields [57],

$$S_{\text{TDBI}} \approx S_{\text{TDBI}}^{(0)} + S_{\text{TDBI}}^{(1)}, \quad (2.8)$$

$$S_{\text{TDBI}}^{(0)} = -M_p^3 N_c N_f \int d^5 x V_{f0}(\phi) e^{-\tau^2} \sqrt{-\det \tilde{g}}, \quad (2.9)$$

$$S_{\text{TDBI}}^{(1)} = -M_p^3 N_c \int d^5 x V_{f0}(\phi) e^{-\tau^2} \sqrt{-\det \tilde{g}} \text{tr} \left[\frac{1}{2} \kappa(\phi) \tau^2 (\tilde{g}^{-1})^{MN} A_M A_N \right. \\ \left. - \frac{1}{8} w(\phi) (\tilde{g}^{-1})^{MN} (\tilde{g}^{-1})^{PQ} \left(F_{NP}^{(L)} F_{QM}^{(L)} + F_{NP}^{(R)} F_{QM}^{(R)} \right) \right], \quad (2.10)$$

where $A_M = A_M^L - A_M^R$ and \tilde{g} is the effective open string metric for the background,

$$\tilde{g}_{MN} = g_{MN} + \kappa(\phi) (\tau')^2 \delta_M^r \delta_N^r. \quad (2.11)$$

Expanding the action to first nontrivial order in the gauge fields also removes an ambiguity of the DBI expression (2.5): As the non-Abelian gauge fields do not commute, one would need to prescribe in which order to take the trace over them. In eq. (2.10) this ambiguity is resolved as there are only two flavored fields in the trace.

Finally, for the TCS term, we employ the expression provided in ref. [53], which generalizes the term derived in ref. [55]. The general expression for the TCS term is complicated, including both a five-dimensional ‘‘bulk’’ term, a closed term, and a boundary term. The two latter terms are the same as those found in QCD by using the flavor anomalies [58–60]. However, we will only need the bulk term here; for the discussion of the boundary terms see ref. [61]. Inserting the Ansatz given above, the only relevant terms turn out to be

$$S_{\text{TCS}} = \frac{iN_c}{4\pi^2} \int \Omega_5^s, \quad (2.12)$$

$$\Omega_5^s = \frac{1}{24} F_1(\tau) \text{tr} \left[A \wedge A \wedge A \wedge \left(F^{(L)} + F^{(R)} \right) \right] \\ - \frac{i}{24} F_3(\tau) \text{tr} \left[A \wedge \left(F^{(L)} - F^{(R)} \right) \wedge \left(F^{(L)} - F^{(R)} \right) \right], \quad (2.13)$$

where $A = A^L - A^R$ is a 1-form and both functions F_1 and F_3 need to approach unity at the boundary for full consistency with the flavor anomalies; they should vanish at large values of τ in order to avoid unphysical IR contributions to the action [53]³.

For the final choice of the functions F_1 and F_3 , we take the result from the flat space analysis [55], but allow a small modification [57, 54] in the choice of the rescaling of the tachyon dependence, in order to better reproduce the properties of dense nuclear matter. Explicitly, this choice is given by

$$F_1(\tau) = e^{-b_1 \tau^2} (1 - 2b_1 \tau^2), \quad F_3(\tau) = e^{-b_3 \tau^2}, \quad (2.14)$$

where the positive parameters b_1 and b_3 reflect the choice of scaling. Note that the choice of the TCS term leaves intact the fit of the background and the physics of the quark phase, for which the instanton number vanishes and the TCS term evaluates to zero.

³The mapping between functions F_i here and the functions f_i in this reference is $F_1 = 12(-f_1 + 2if_2 - f_3)$, $F_3 = 12(f_3 - f_1)$.

To summarize, the full action governing the background (metric, dilaton and the tachyon) is then given by

$$S_{\text{bg}} \equiv S_g + S_{\text{GH}} + S_{\text{TDBI}}^{(0)} \quad (2.15)$$

in eqs. (2.2), (2.3), and (2.9), whereas the probe gauge fields are described by

$$S_{\text{gf}} \equiv S_{\text{TDBI}}^{(1)} + S_{\text{TCS}} \quad (2.16)$$

in eqs. (2.10) and (2.13).

To build hybrid equations of state we need to choose a procedure to match the holographic and low-energy equations. We will present two procedures different in spirit, which we will refer to as procedures (a) and (b) from now on:

- (a) Choose a phenomenologically reasonable density n_t at which to perform the matching, and introduce a rescaling parameter c_b of the flavor action to obtain realistic pressure scales by replacing $S_{\text{TDBI}}^{(1)} \mapsto c_b S_{\text{TDBI}}^{(1)}$ and $S_{\text{TCS}} \mapsto c_b S_{\text{TCS}}$. We then choose b_1, c_b in order to obtain an equation of state with continuous pressure, baryon number density and energy density. This is exactly the same approach followed in refs. [33, 34], and essentially introduces a new parameter in an attempt to correct for the various approximations of the holographic model. This procedure tends to produce the most phenomenologically reasonable equations of state, at the price of losing predictability and control over the areas of the model that would require refinement.
- (b) Fit the model to properties of nuclear matter at saturation, then determine the transition between the two equations of state by requiring continuity of pressure and baryon number density. This is exactly the same approach as that followed in ref. [26]. To do so, we fit b_1 to have the model-determined baryonic saturation density n_0 coincide with the phenomenological value $n_S = 0.16\text{fm}^{-3}$. This procedure tends to produce less reliable equations of state, with some unphysical features, such as a first-order phase transition at densities around saturation, while focusing on retaining control over the qualitative features of the holographic method, in particular highlighting the degree of failure of the homogeneous Ansatz at lower densities.

For both procedures, we will use the holographic equation of state obtained with two different background choices, commonly labeled as 5b and 7a (see App. A of ref. [34] and App. B of ref. [57] for details on the definitions). These models were determined primarily by comparing to available the lattice data for the thermodynamics of QCD. There are also other fits of the V-QCD model available [62, 54], which also take into account data for particle spectra, but produce a less precise description of the finite temperature lattice data. For low-energy equations of state, we use the three variants from Hebel-Lattimer-Pethick-Schwenk [63], and SLy4 [64, 65]. We will perform procedure (a) for three values of n_t , namely $\{1.2, 1.5, 1.8\}n_S$, for a total of 30 different equations of state, where n_S is the phenomenological saturation density (the soft and intermediate EOS from ref. [63] result in a single hybrid EOS for procedure (b)).

3 Symmetric nuclear matter

To describe dense nuclear matter we employ the framework usually referred to as the “homogeneous Ansatz”. It consists in assuming the gauge fields only depend on the holographic coordinate r : This can be thought of as being the result of smearing a large number of instantons (each carrying unit baryon number) over \mathbb{R}^3 , and the field configuration inherits many similarities with the single instanton in singular gauge, despite a rigorous derivation is still not available.

The first step is to set $N_f = 2$ and employ the only consistent homogeneous Ansatz for the fields $A_{L/R}^i$, given by [66, 50, 30, 57]:

$$A_i^L = -A_i^R = -\frac{H(r)}{2}\sigma^i, \quad (3.1)$$

with σ^i , $i = 1, 2, 3$ being the three Pauli matrices. The other field that is turned on in the isospin-symmetric configuration is the Abelian potential $A_t(r)$. The only allowed structure for it is then

$$A_t^L = A_t^R = \frac{\widehat{a}_0(r)}{2}\mathbf{1}. \quad (3.2)$$

With this normalization, the UV value of this field is holographically dual to the quark chemical potential, and it relates to the baryon chemical potential μ_B that couples to the baryon number density as

$$\frac{1}{2}\widehat{a}_0(r=0) \equiv \mu = \frac{1}{N_c}\mu_B. \quad (3.3)$$

To compute the baryon number for this configuration (together with the tachyon), we integrate the equation of motion for \widehat{a}_0 obtained from the gauge field action in eq. (2.16). We find [57]

$$N_B = -\frac{1}{4\pi^2} \int d^3x \, dr \frac{d}{dr} [F_1(\tau(r))H(r)^3]. \quad (3.4)$$

We see that N_B vanishes for every smooth profile $H(r)$ since $H(r=0) = 0$ to have a finite energy configuration [66]. A way to retain both a finite nonvanishing baryon number and the homogeneous field configuration is to allow the function $H(r)$ to have discontinuities [50]: The simplest choice is for it to have a discontinuity in the bulk at some finite $r = r_c$ (that will be determined by extremizing the action), and have $H(r > r_c) = 0$. This roughly corresponds to placing the instantons at $r = r_c$ before the smearing procedure. Analogously to the baryons/instantons forming a lattice in the holographic direction following “popcorn transitions” [67, 68], the function $H(r)$ can in principle have multiple discontinuities (see ref. [69]), a refinement we do not include in the present work.

Other components of the gauge field vanish due to the absence of sources, and we are then left with two ODEs for $H(r), \widehat{a}_0(r)$ to be solved numerically, which we choose to do

using a shooting method. A convenient choice is to shoot from the IR, since we can then fix the baryon number density n_B and use it to impose the Dirichlet boundary condition

$$H(r = r_c)^3 = -\frac{4\pi^2 n_B}{F_1(\tau(r_c))}. \quad (3.5)$$

The vanishing of boundary terms in the variation of the action imposes Neumann boundary conditions for $\widehat{a}_0(r_c)$, and fixes the derivative $H'(r_c)$ as a function of $H(r_c)^2$ [61]:

$$4\pi^2 M_p \left(\frac{e^{2A(r)} V_f(\phi, \tau) w(\phi)^2}{\sqrt{e^{2A(r)} + \kappa(\phi) \tau'^2}} H' \right)_{r=r_c} = (\widehat{a}_0 F_1(\tau) H^2)_{r=r_c}. \quad (3.6)$$

The value of $\widehat{a}_0(r_c)$ necessary to impose $H(r = 0) = 0$ thus becomes the only shooting parameter. The procedure of determining r_c is made easy by this choice of shooting method: The variation of the on-shell action with respect to r_c in our setup with a single discontinuity and vanishing fields for $r > r_c$, is given by the Lagrangian density evaluated at r_c . It thus suffices to numerically solve the algebraic equation $\mathcal{L}(r = r_c) = 0$ for each choice of shooting parameter.

The saturation density n_0 can be derived from the model by finding the onset of baryonic matter at which the grand potential for nuclear matter vanishes, $\Omega(n_0) = 0$. Through the rest of this work, we will keep separated the concepts of the model-derived saturation density n_0 and the phenomenological saturation density n_S . The value of the former is determined by the choice of b_1 and is subject to an intrinsic error introduced by the assumption of homogeneity, while the value of the latter is the observed one of $n_S = 0.16 \text{fm}^{-3}$. When following procedure (b), the value of b_1 is chosen by requiring $n_0 = n_S$, while for procedure (a) the two values in general do not coincide. Since procedure (a) is developed with the scope of matching the holographic EOS with other phenomenological ones at densities higher than saturation, then it is not a severe problem that in this case $n_0 \neq n_S$.

4 Isospin asymmetry

The introduction of isospin asymmetry is performed by turning on a nonvanishing isospin chemical potential μ_I . This is done according to the standard holographic dictionary by imposing the UV boundary condition on $(A_t^{L/R})^a$:

$$A_t^L(r = 0) = A_t^R(r = 0) = \frac{\mu_I}{2} \sigma^3, \quad (4.1)$$

where we have aligned the group direction σ^3 with the third component of the isospin.

The boundary condition turns on components of the gauge field that could be set to zero in the symmetric case, in particular it turns on $(A_t^{L/R})^{a=3}$, $\widehat{A}_3^{L/R}$ and partially removes the symmetry of the field $A_i^{L/R}$. The new self-consistent Ansatz for the isospin asymmetric

setup is then given by:

$$A_i^L = -A_i^R = -\frac{H(r)}{2}\sigma^i, \quad \text{with } i = 1, 2 \quad (4.2)$$

$$A_3^L = -A_3^R = -\frac{H_3(r)}{2}\sigma^3 - \frac{L_3(r)}{2}\mathbb{1}, \quad (4.3)$$

$$A_i^L = A_i^R = a_0(r)\sigma^3 + \frac{\widehat{a}_0}{2}\mathbb{1}. \quad (4.4)$$

The other components allowed in principle by the symmetries (the Abelian component for A_1, A_2 and the missing non-Abelian components A_i^1, A_i^2 , on top of terms involving the antisymmetric symbol ϵ^{ij}) are unsourced and vanishing due to the equations of motion.

The UV boundary conditions are again obtained by requiring the vanishing of the sources on the field theory side except for the chemical potentials, so we have

$$H(r=0) = H_3(r=0) = L_3(r=0) = 0, \quad (4.5)$$

$$\widehat{a}_0(r=0) = 2\mu, \quad (4.6)$$

$$a_0(r=0) = \frac{\mu I}{2}. \quad (4.7)$$

The IR boundary conditions instead are read off the boundary terms that remain when performing the variation of the action and imposing the equations of motion:

$$\widehat{a}'_0(r_c) = 0, \quad L'_3(r_c) = 0, \quad (4.8)$$

$$24\pi^2 M_p^3 \left(\frac{e^{2A(r)} V_f(\phi, \tau) w(\phi)^2}{\sqrt{e^{2A(r)} + \kappa(\phi) \tau'^2}} a'_0 \right)_{r=r_c} = [(F_1(\tau) + 2F_3(\tau)) H^2 L_3]_{r=r_c}, \quad (4.9)$$

$$4\pi^2 M_p^3 \left(\frac{e^{2A(r)} V_f(\phi, \tau) w(\phi)^2}{\sqrt{e^{2A(r)} + \kappa(\phi) \tau'^2}} H' \right)_{r=r_c} = H(\widehat{a}_0 F_1(\tau) H_3 - 2a_0 F_3(\tau) L_3)_{r=r_c}, \quad (4.10)$$

$$4\pi^2 M_p^3 \left(\frac{e^{2A(r)} V_f(\phi, \tau) w(\phi)^2}{\sqrt{e^{2A(r)} + \kappa(\phi) \tau'^2}} H'_3 \right)_{r=r_c} = (\widehat{a}_0 F_1(\tau) H^2)_{r=r_c}. \quad (4.11)$$

To work at a fixed baryonic density we impose the condition

$$H_3(r_c) H(r_c)^2 = -\frac{4\pi^2 n_B}{F_1(\tau(r_c))}, \quad (4.12)$$

which in the symmetric case was enough to fix the IR value $H(r_c)$, but now only provides a relation between $H_3(r_c)$ and $H(r_c)$. For the shooting method we use the parametrization $H_3(r_c) = \delta_H H(r_c)$, where we have introduced the parameter δ_H being the ratio of the third and the other components on the boundary. In the symmetric scenario $\delta_H = 1$, but in the asymmetric case it is treated as a shooting parameter that is fixed by the conditions (4.5).

4.1 Small isospin approximation: Symmetry energy

We will now compute the symmetry energy of the system. For homogeneous nuclear matter it is defined as the coefficient of the quadratic term in the expansion of the energy per nucleon in the asymmetry parameter $\beta = (N - Z)/A$:

$$\frac{\mathcal{E}}{n_B}(n_B, \beta) = \frac{\mathcal{E}_0}{n_B}(n_B, 0) + S_N(n_B)\beta^2 + \dots \quad (4.13)$$

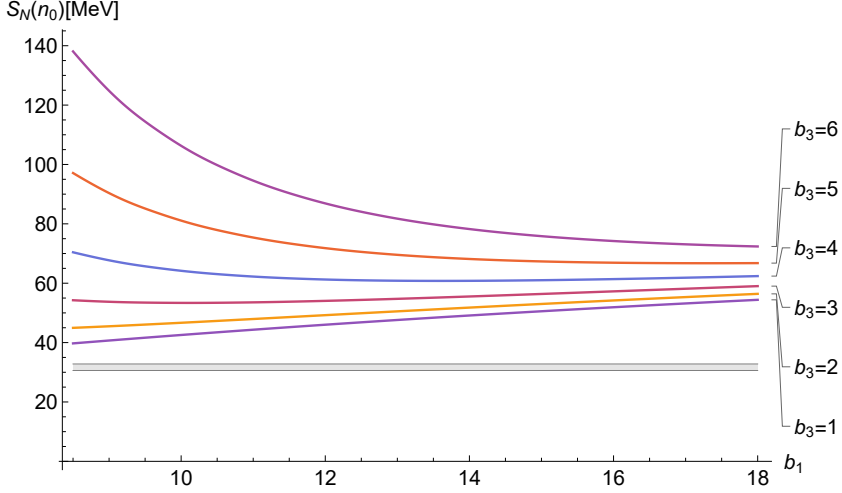


Figure 1. Symmetry energy at saturation density n_0 (as determined by the model) as a function of b_1 for various values of b_3 . In gray the phenomenologically measured value including its experimental error.

It is indeed possible to compute $S_N(n_B)$ from the above expansion by using that $n_I = \frac{\partial \mathcal{E}}{\partial \mu_I}$:

$$S_N(n_B) = \frac{n_B}{8} \left. \frac{\partial \mu_I}{\partial n_I} \right|_{n_I=0}, \quad (4.14)$$

as well as the nuclear physics convention assigning isospin number $+\frac{1}{2}$ ($-\frac{1}{2}$) to the proton (neutron).

It is, however, more convenient to exploit the fact that the computation has to be done around the isospin symmetric configuration, so that we can linearize the μ_I -dependence of the fields and drop higher-order corrections. Let us explicitly manifest the linear μ_I dependence of the fields via the expansion:

$$a_0(r) = \tilde{a}_0(r)\mu_I + \mathcal{O}(\mu_I^2), \quad (4.15)$$

$$L_3(r) = \tilde{L}_3(r)\mu_I + \mathcal{O}(\mu_I^2), \quad (4.16)$$

$$H_3(r) = H(r) + \mathcal{O}(\mu_I^2), \quad (4.17)$$

where the functions $\tilde{a}_0(r)$ and $H(r)$ receive corrections only at order $\mathcal{O}(\mu_I^2)$ (consistent with the equations of motion).⁴

Plugging this expansion into the action, we have:

$$\Omega = -\mathcal{E}_0(n_B) - \frac{1}{2}\Lambda(n_B)\mu_I^2, \quad n_I = -\frac{\partial \Omega}{\partial \mu_I} = \Lambda(n_B)\mu_I, \quad (4.18)$$

⁴This setup is equivalent to that of ref. [41]. The approximation of small μ_I is equivalent to that of slow and rigid rotation in SU(2). The two descriptions are in fact connected by a gauge transformation; see App. A of ref. [41].

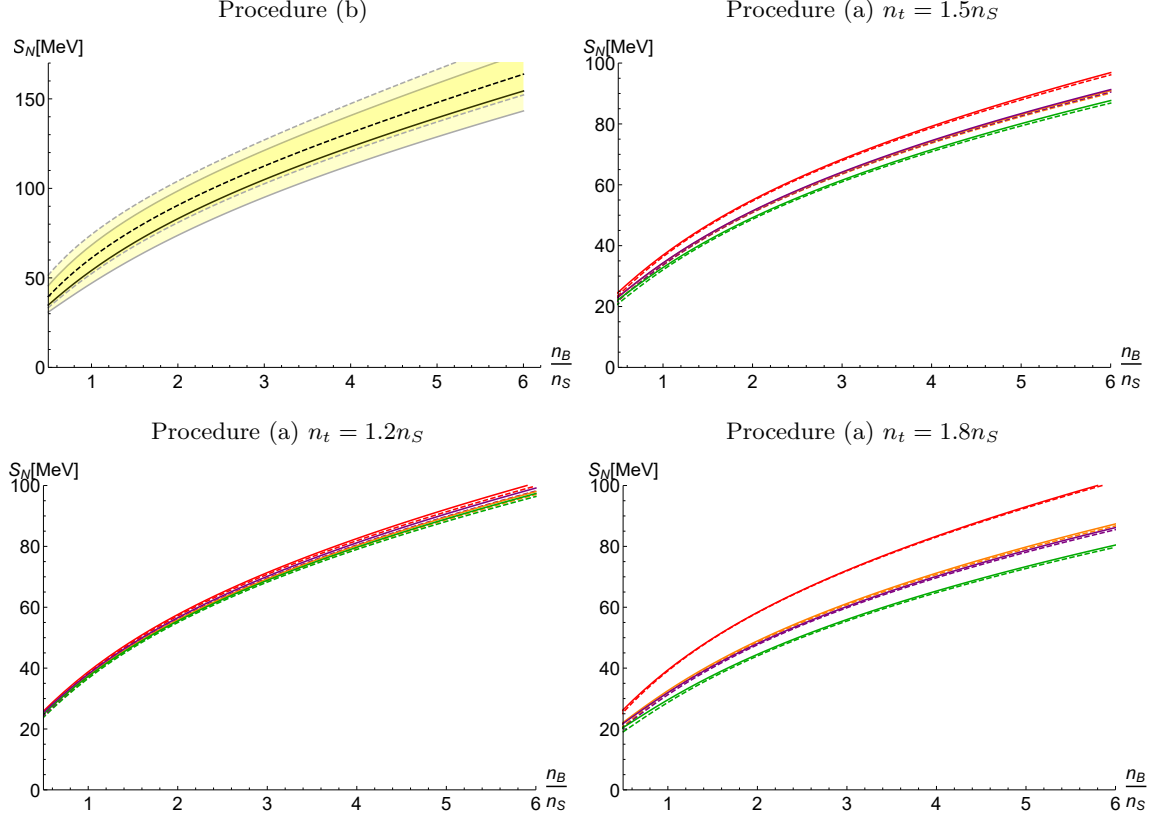


Figure 2. The symmetry energy as a function of density measured in units of the saturation density n_S . Top left panel: Matching procedure (b): A yellow band spanning the values $b_1 \in [12, 22]$ with gray boundaries is presented; the black curves correspond to the physical saturation density. Remaining panels: Matching procedure (a) with matching density n_t . The color coding is: Green for HLPS soft, orange for HLPS intermediate, red for HLPS stiff, purple for SLy4. Solid (dashed) lines correspond to the choice of V-QCD potentials 7a (5b).

where we have introduced the functions $\mathcal{E}_0(n_B)$, $\Lambda(n_B)$ defined by the integrals

$$\mathcal{E}_0(n_B) \equiv M_p^3 N_c \int_0^{r_c} dr \frac{V_f(\phi, \tau)}{4\sqrt{e^{2A(r)} + \kappa(\phi)\tau'^2}} \left[3 \left(e^{2A(r)} + \kappa(\phi)\tau'^2 \right) w(\phi)^2 H^4 + 12e^{2A(r)} \kappa(\phi)\tau^2 \left(e^{2A(r)} + \tau'^2 \right) H^2 + e^{2A(r)} w(\phi)^2 \left(3H'^2 + \tilde{a}_0'^2 \right) \right], \quad (4.19)$$

$$\Lambda(n_B) \equiv 2M_p^3 N_c \int_0^{r_c} dr \frac{V_f(\phi, \tau)}{4\sqrt{e^{2A(r)} + \kappa(\phi)\tau'^2}} \left[e^{2A(r)} w(\phi)^2 \left(4\tilde{a}_0'^2 + \tilde{L}_3'^2 \right) + 4 \left(e^{2A(r)} + \kappa(\phi)\tau'^2 \right) \left(2w(\phi)^2 H^2 \tilde{a}_0'^2 + e^{2A(r)} \kappa(\phi)\tau^2 \tilde{L}_3'^2 \right) \right]. \quad (4.20)$$

With the definition of n_I obtained in eq. (4.18) we can readily obtain the expression for the symmetry energy via eq. (4.14):

$$S_N(n_B) = \frac{n_B}{8\Lambda(n_B)}. \quad (4.21)$$

Moreover, since $n_I = \Lambda\mu_I$ due to the above arguments, and since n_I also has to be determined by the near-boundary behavior of the field \tilde{a}_0 due to the field-operator holographic map, we conclude that it is not necessary to explicitly compute the integral (4.20), but it is sufficient to compute $\Lambda(n_B)$ as

$$\Lambda(n_B) = -M_p^3 N_c \left(\frac{e^{2A(r)} V_f(\phi, \tau) w(\phi)^2}{\sqrt{e^{2A(r)} + \kappa(\phi) \tau'^2}} \tilde{a}'_0 \right) \Big|_{r \rightarrow 0}. \quad (4.22)$$

In this analysis, we have not considered the possibility of a contribution to S_N arising from the change of the location at which the discontinuity is placed, induced by μ_I ; that is, we determine the position in the bulk by solving $L(r_c) = 0$ at the zeroth order in μ_I . It can be proven that the perturbation of the Lagrangian induces a perturbation of r_c quadratic in μ_I , so one may wonder if this perturbation allows the unperturbed Lagrangian to contribute to S_N : It can, however, be shown by using the definition of r_c that this contribution vanishes due to the equations of motion. Thus, the isospin-induced correction to r_c can only contribute to a higher order in μ_I , see App. A.

Near saturation density it is useful to define the parameters S_0, L, K_{sym} :

$$S_N(n_B) = S_0 + \frac{1}{3} L \frac{n_B - n_S}{n_S} + \frac{1}{18} K_{\text{sym}} \left(\frac{n_B - n_S}{n_S} \right)^2 + \dots \quad (4.23)$$

We have explored the symmetry energy's ($S_N(n_0)$) dependence on b_1 and b_3 at $c_b = 1$, summarized in fig. 1. $S_N(n_0)$ is an increasing function of b_3 at fixed b_1 . Moreover, in the range of b_1 relevant to our matching procedures, $S_N(n_0)$ is already overestimated for the flat space expression of the TCS term [55] corresponding to $b_3 = 1$, that is, the physics of isospin asymmetry is better described for small values of b_3 . This is in stark contrast with the preferred values of b_1 , which governs instead the onset of nuclear matter. A minimal choice in modifying the flat space expression ($b_1 = b_3 = 1$) for S_{TCS} would be to choose a single rescaling for both functions F_1, F_3 , so that $b_1 = b_3 = b$. However, this would lead to a very large symmetry energy for both of our matching procedures (and consequently very high proton fractions for the nuclear matter in β -equilibrium). We have thus for phenomenological reasons fixed $b_3 = 1$, so that the rescaling only affects the function $F_1(\tau)$, to keep the number of free parameters in the model to a minimum. Without the introduction of the rescaling parameter c_b (as in procedure (b)), this still leads to large symmetry energies, but remarkably the results for procedure (a) turns out to be close to (and often in fact compatible with) phenomenology⁵.

In fig. 2 is shown the symmetry energy, $S_N(n_B)$, for each combination of matching procedure, potential, and parameters c_b and b_1 , which is computed as the coefficient of the expansion around saturation density (see App. B for the values of the parameters for the matching procedure (a)). The symmetry energy at saturation density resulting from matching procedure (a) lies in the range $S_0 \in [28.7, 39.4]$ MeV. Breaking down this result in

⁵It is possible that an appropriate modification of the functional form of F_3 (and F_1) may make the model reproduce phenomenological values of the symmetry energy as well as baryon onset, *without* the introduction of the rescaling parameter c_b . This will be beyond the scope of the present paper.

the various EOSs, we find that the soft one has $S_0 \in [28.7, 37.3]$ MeV, the intermediate $S_0 \in [31.9, 37.6]$ MeV, the one matched with SLy4 $S_0 \in [31.3, 38.0]$ MeV and the stiff one $S_0 \in [36.4, 39.4]$ MeV. The lower (upper) bounds always correspond to EOS whose holographic part is built with the 5b (7a) background. Moreover, the parameter L of the expansion around saturation lies in the range $L \in [51.6, 71.0]$ MeV, with the upper (lower) bound corresponding again to the EOS from the 5b (7a) background. Both values are in good agreement (on the larger side) with phenomenology, a nontrivial result given the matching procedure: The rescaling with c_b not only provides continuous EOSs, but also rescales the symmetry energy and its derivative with respect to the density to their phenomenological values. For the quantity K_{sym} , the model predicts values $K_{\text{sym}} \in [-106.1, -42.9]$ MeV.

A very interesting result that we will obtain in the following sections is that the EOSs that have S_0 close to phenomenology are also those that result in neutron stars more prone to satisfying the observational bounds. This is also a nontrivial result and may hint that the rescaling procedure is not as bad a correction to the many approximations employed here as it may seem.

4.2 General configuration: β -equilibrated neutral matter

The approximation presented in the previous section is only reliable in the limit of small isospin chemical potential: This is enough to compute the symmetry energy, but not to determine the equation of state for β -equilibrated matter. The regimes of β -equilibrium and charge neutrality tend, in fact, to produce neutron-rich matter, which then translates into a regime of large (negative in our conventions) isospin.

If our goal is to describe neutron-rich matter in the core of neutron stars, we need to solve the full isospin-dependent problem described by the Ansatz in eqs. (4.2), (4.3) and (4.4).

While in the general configuration baryon and isospin number densities are independent, we impose β -equilibrium in the system by introducing negatively charged leptons. This introduces a new parameter to the problem, the chemical potential of leptons μ_l with $l = e, \mu$ for electrons and muons. The system is then constrained again to a single degree of freedom by imposing electric charge neutrality.

The two conditions are given by

$$\mu_l = \mu_N - \mu_P = -\mu_I, \quad (4.24)$$

$$\frac{1}{2}n_B + n_I = \sum_l n_l, \quad (4.25)$$

where μ_N, μ_P are the chemical potentials of the neutron and the proton, respectively, and n_l is the lepton number density. The leptonic free energy is that of a (massive) Fermi gas:

$$\Omega_\ell = -\frac{1}{24\pi^2} \Theta(\mu_\ell - m_\ell) \left[(2\mu_\ell^2 - 5m_\ell^2) \mu_\ell \sqrt{\mu_\ell^2 - m_\ell^2} + 3m_\ell^4 \log \left(\frac{\sqrt{\mu_\ell^4 - m_\ell^4} + \mu_\ell}{m_\ell} \right) \right], \quad (4.26)$$

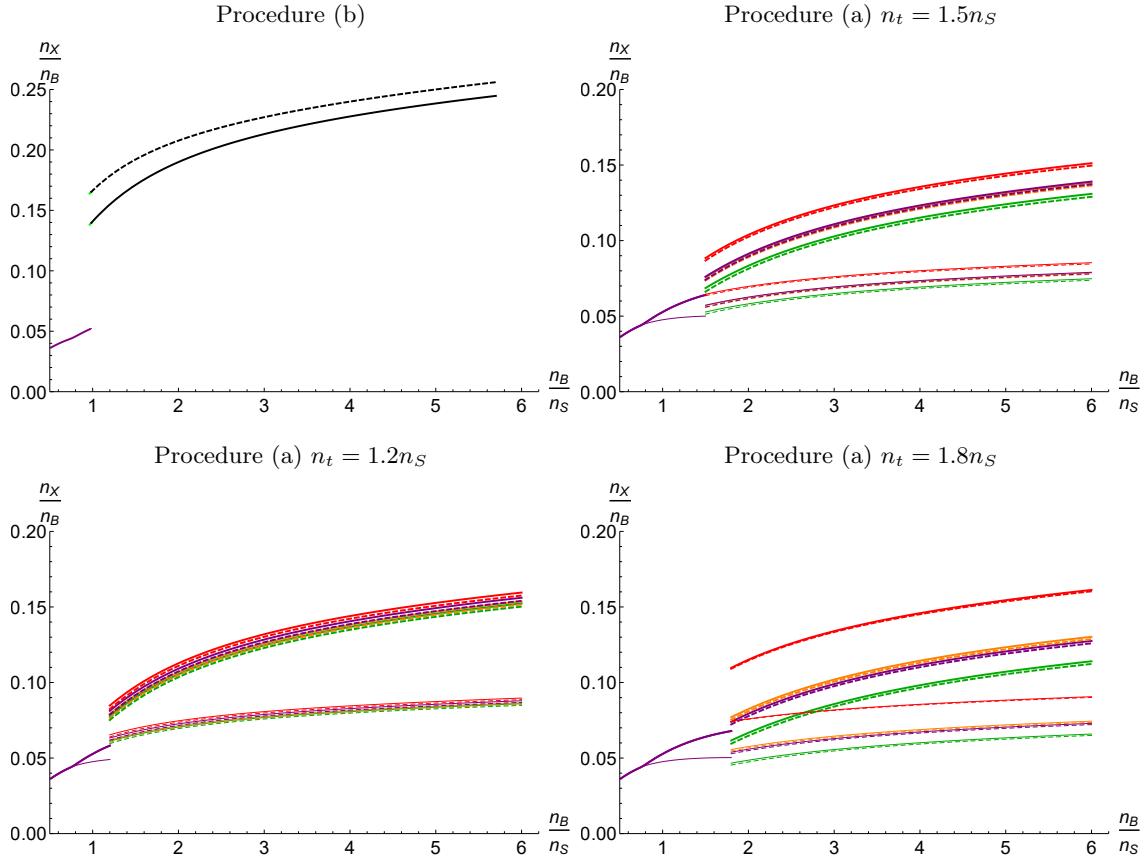


Figure 3. Particle fractions as functions of density in units of the saturation density. Top left panel: Matching procedure (b). Remaining panels: Matching procedure (a) with matching density n_t . For the color coding, see fig. 2. Thick lines represent proton fractions, while thin lines (always below the thick ones) represent electron fractions: Muon fractions can be easily derived as the difference between the two, as dictated by charge neutrality, and neutron fractions are simply given by subtracting the proton fractions from unity. For every plot we also show in purple the proton fractions predicted by the SLy4 EOS at densities lower than the matching density.

from which we can obtain the leptonic density as a function of the chemical potential:

$$n_\ell(\mu_\ell) = \Theta_H(\mu_\ell - m_\ell) \frac{(\mu_\ell^2 - m_\ell^2)^{\frac{3}{2}}}{3\pi^2}. \quad (4.27)$$

Plugging eqs. (4.27) and (4.24) into eq. (4.25) yields:

$$\frac{1}{2}n_B + n_I - \frac{|\mu_I|^3}{3\pi^2} \left[\Theta_H(-\mu_I - m_\mu) \left(1 - \frac{m_\mu^2}{\mu_I^2} \right)^{\frac{3}{2}} + \Theta_H(-\mu_I) \right] = 0, \quad (4.28)$$

where we have approximated the electron to be massless. The isospin charge density is obtained from the near-boundary behavior of $a'_0(z)$, which is determined by the parameters n_B , μ_I , so that solving eq. (4.28) provides $\mu_I(n_B)$.

Having now a family of solutions determined by the single parameter⁶ n_B , we can proceed to compute the equation of state.

⁶Note, however, that eq. (4.28) is derived assuming that the parameters n_B and n_I are read off of the

To do so we compute the energy density \mathcal{E} and pressure P of the system. For a homogeneous system, the pressure is given in terms of the free energy Ω as $P = -\Omega$. For the leptons, the free energies Ω_e, Ω_μ are given by eq (4.26), while for the baryonic matter we can employ the holographic map to identify the free energy Ω_b with:

$$\Omega_b = - \left(S_{TDBI}^{on-shell} + S_{TCS}^{on-shell} \right). \quad (4.29)$$

The total pressure is then given by:

$$P = -\Omega_b - \Omega_e - \Omega_\mu, \quad (4.30)$$

while the total energy density is obtained by accounting for the chemical potentials and number densities as:

$$\mathcal{E} = -P + \mu_B n_B + \mu_I n_I + \mu_e n_e + \mu_\mu n_\mu. \quad (4.31)$$

While this is sufficient to compute the EOS for the baryonic phase above the transition density n_t , it does not account yet for the possibility of a quark matter phase, which will be discussed in the next section.

Another quantity that can be computed from the solution of the β -equilibrium is the proton fraction (and the fractions of other particles) as a function of density, see fig. 3. As a direct consequence of the smaller (and more realistic) symmetry energy of the EOS obtained via matching procedure (a), the corresponding proton fractions are also lower, and the gap between them and realistic ones (in the plot obtained from the SLy4 EOS) gets smaller for softer hybrid EOS. This trend is consistent with the results we will obtain for mass-radius (MR) curves of neutron stars: Matching the V-QCD-derived EOS with softer ones produces more phenomenologically acceptable MR curves when the matching is performed at transition densities n_t in the range $n_t \in [1.2n_S, 1.8n_S]$.

5 Quark phase

The onset of quark matter can be a decisive factor in establishing the highest mass a neutron star can achieve. If we want to compare our result with observations, we need to account for the possibility of quark matter influencing the MR curves of neutron stars. To model the dense quark-matter phase, we follow [18, 19] and compute the equation of state from the thermodynamics of charged black hole solutions in V-QCD. For this computation, we need to include the effects of backreaction of the gauge fields onto the geometry: To turn on a nontopological charge density, a horizon in the background is needed to impose Dirichlet boundary conditions on the Abelian vectorial gauge field \hat{A}_t . Other components

asymptotics of the A_t field rescaled with the overall coefficient of the action, as per standard holographic dictionary: This implies that for matching procedure (a), they both get rescaled with c_b . Because of this, the equation of state will now depend from c_b in a nontrivial way: Before the introduction of β -equilibrium, it amounts to an overall rescaling of density, energy and pressure. We are considering now to have already fixed c_b, b_1 to the values appropriate for the matching, while practically the procedure involves solving eq. (4.28) at a fixed matching density for many values of (b_1, c_b) and determining the pairs that produce a continuous equation of state after matching.

of the gauge field are set to zero. For the metric, we take the Ansatz of eq. (2.4) but instead of setting the blackening factor $f(r)$ to one it is now a free function. We find the solution that describes a geometry with a planar horizon ($f(r_h) = 0$ for some value of $r = r_h$) by numerically solving the equations of motion arising from the gluon and flavor actions in eqs. (2.2) and (2.5). For the potentials we are using, only a “hairless” chirally symmetric black hole phase solution appears, so that the tachyon field T vanishes. This solution is dual to a chirally symmetric quark-gluon plasma.

At zero quark masses, and accounting for the presence of the strange quark, β -equilibrium is trivially solved by an isospin symmetric configuration $n_u = n_d = n_s$, setting $\mu_I = 0$ and similarly having vanishing lepton number densities. This is of course an approximation, in reality we should account for quark masses, including the larger strange mass. The onset of the quark phase is then uniquely determined by requiring continuity of the pressure and baryon number chemical potential μ_B at the transition, while the baryon number density is in general discontinuous. We follow the approach [57, 33, 34] where the pressure from nuclear matter is directly compared to the pressure of quark matter (or, more precisely, the pressure difference between the quark matter and the vacuum) despite the fact that the nuclear matter pressure was computed in the probe approximation whereas the quark matter solution is fully backreacted.

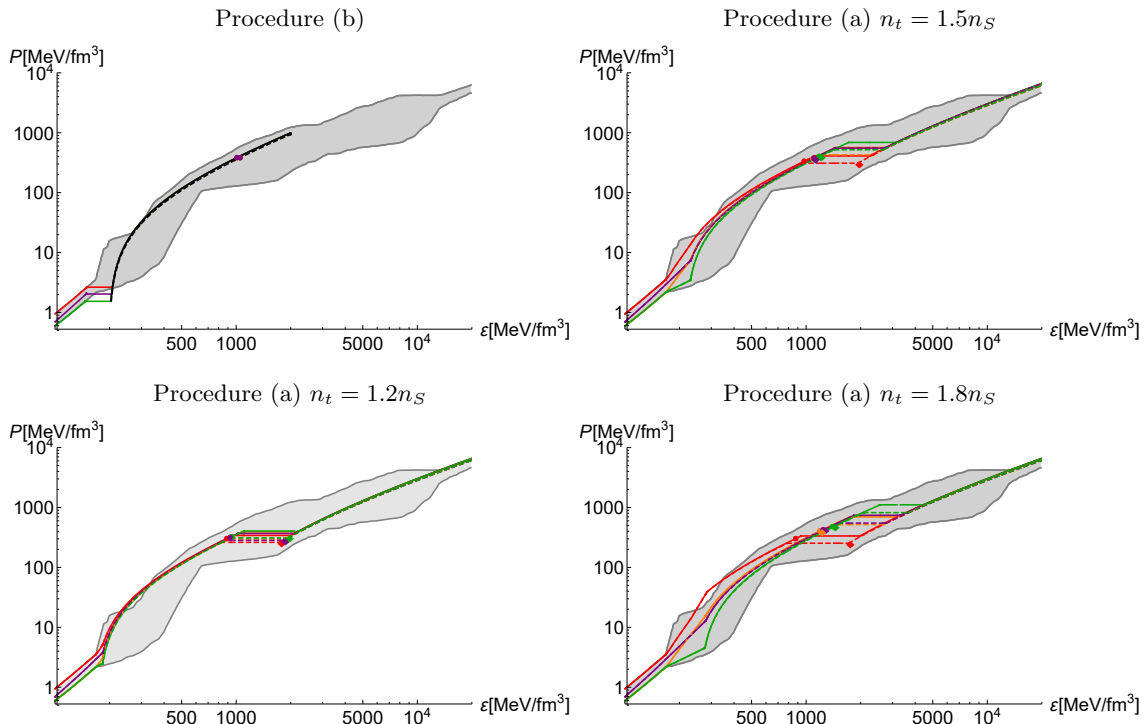


Figure 4. Collection of equations of state. Top left panel: Matching procedure (b), the black part of the curves is derived from V-QCD and coincides for all the choices of low density EOS. Remaining panels: Matching procedure (a) with matching density n_t . For the color coding, see fig. 2. For each solid (dashed) curve and for each color, a colored dot (diamond) corresponds to the central pressure and energy density of the heaviest neutron star that the EOS supports.

In fig. 4 we present the hybrid equations of state built with the methodology described

for each combination of matching procedure, potential, low density behavior and transition density, for a total of 30 equations.

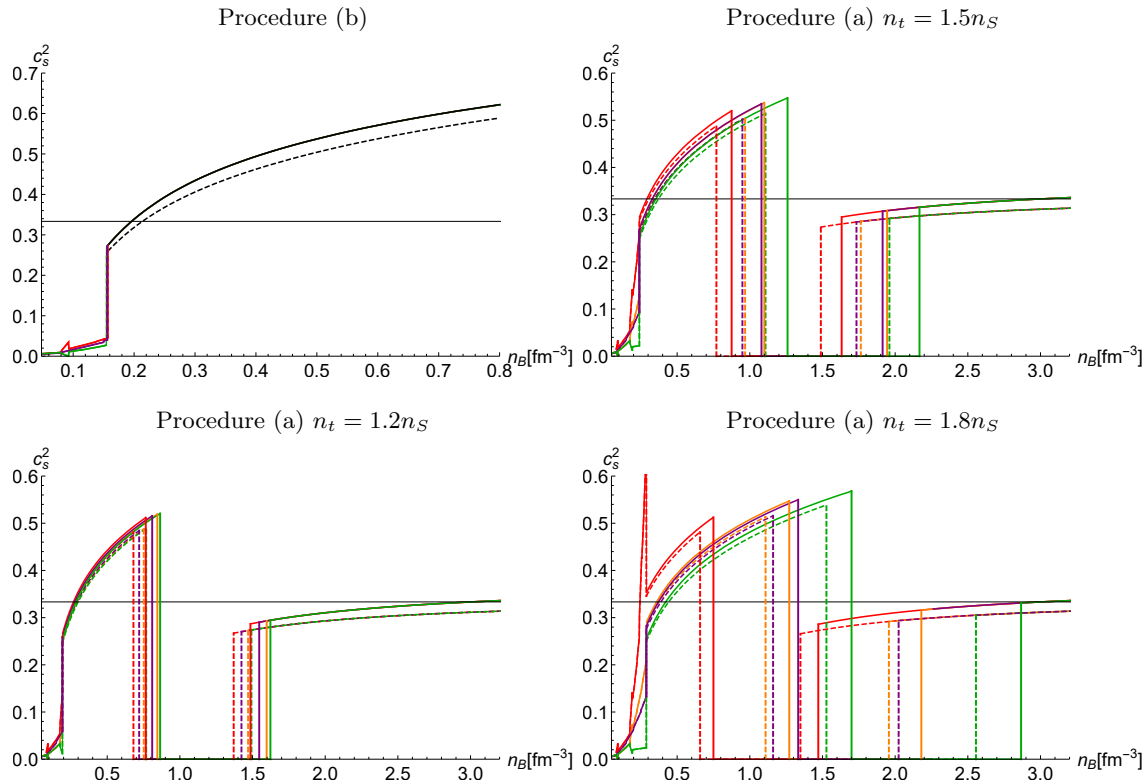


Figure 5. Speed of sound squared as a function of baryonic density. Top left panel: Matching procedure (b). Remaining panels: Matching procedure (a) with matching density n_t . The horizontal gap in these speeds of sound manifests due to the phase transition from baryonic to quark matter. The vertical lines are displayed as guides for the beginning and ending of the gaps. For the color coding, see fig. 2. The horizontal black line marks the conformal value $c_s^2 = 1/3$ for reference.

With the equations of state of fig. 4 in hand, we can compute the speed of sound squared numerically as

$$c_s^2 = \frac{\partial P}{\partial \mathcal{E}}. \quad (5.1)$$

In fig. 5, we display the speed of sound squared for all the EOSs computed, but taking into account also the transition to the quark matter phase, which manifests itself as a horizontal gap in the plots. Note that we could only take the quark matter phase transition into account for the procedure (a).

6 Neutron stars

We want to compute the properties of neutron stars resulting from the set of equations of state that we have built: To do so, we solve the Tolman-Oppenheimer-Volkov (TOV) equations, that describe the coupling between a static, spherically symmetric distribution

of matter and gravity. The set of coupled equations is given by

$$\frac{dP}{dr} = -G(\mathcal{E} + P) \frac{m + 4\pi r^3 P}{r(r - 2Gm)}, \quad (6.1)$$

$$\frac{dm}{dr} = 4\pi r^2 \mathcal{E}. \quad (6.2)$$

The TOV equations can be solved by choosing initial values $P(r = 0) = P_0, m(r = 0) = 0$ and identifying the value R at which $P(R) = 0$ as the radius of the star (correspondingly, the mass of the star is given by $M = m(R)$). Repeating the process for all values of P_0 that result in stable stars leads to a curve in the M - R plane describing all possible neutron stars for each given EOS.

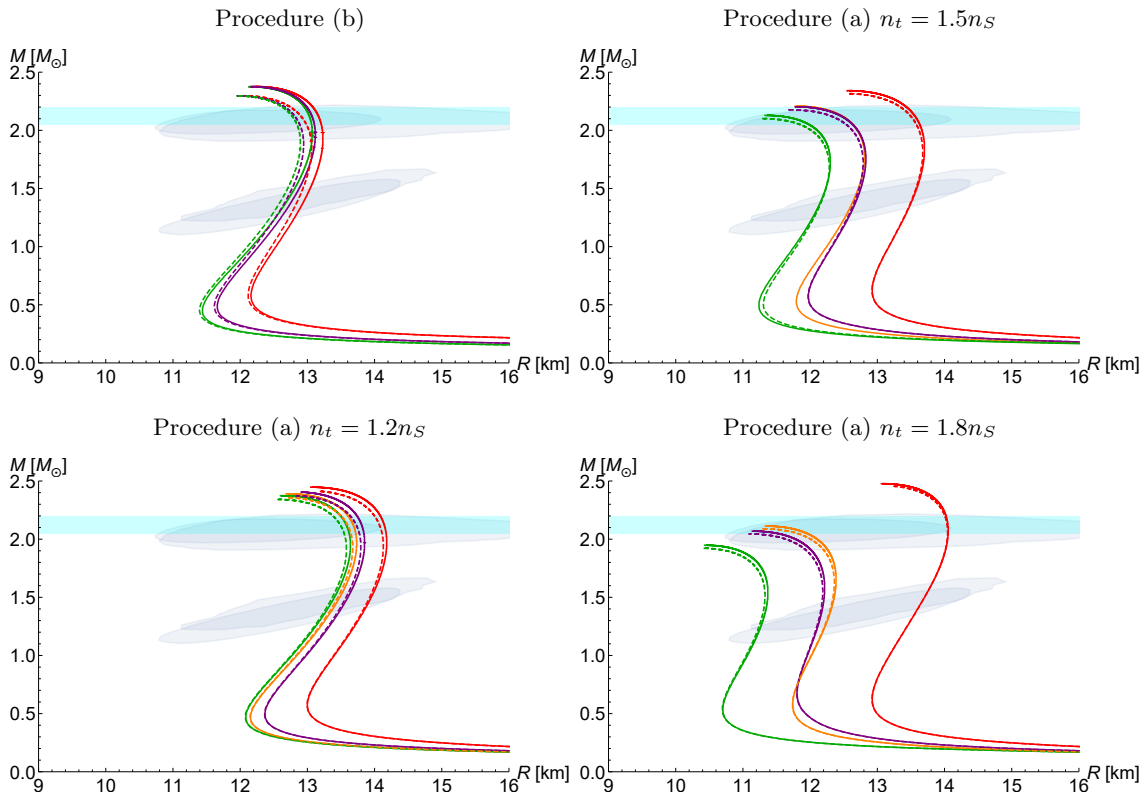


Figure 6. Mass-Radius (MR) curves for neutron stars. Top left panel: Matching procedure (b). Remaining panels: Matching procedure (a) with matching density n_t . For the color coding, see fig. 2.

Our results for this procedure are shown in fig. 6, where we also report the constraints from NICER [70–73] and an estimate on the highest possible mass as determined in ref. [74]. Almost all of our EOSs are stiff enough to reach the range of two solar masses as required, for example, the NICER measurement of the mass of J0740+6620. However, the EOSs with $n_t = 1.8n_S$ and the soft variant of the HLPS EOSs are so soft that they are in tension with this measurement. Moreover, many other EOSs, including all EOSs constructed with the procedure (b), lead to slightly larger maximum masses than the bound of [74]. Note however that this bound is a rather indirect result of the analysis of the GW170817 binary merger event.

Note that none of our equations of state can support stable quark matter cores in neutron stars [34]. However, the detailed picture is different depending on the choice potentials in the V-QCD action. For all of our hybrid EOSs using potentials 7a, as the mass is increased, the star becomes unstable even before the phase transition is reached in the core of the star, while for potentials 5b the phase transition happens at a lower energy density, so that the transition is reached in the cores of the heaviest neutron stars constructed from six equations of state.

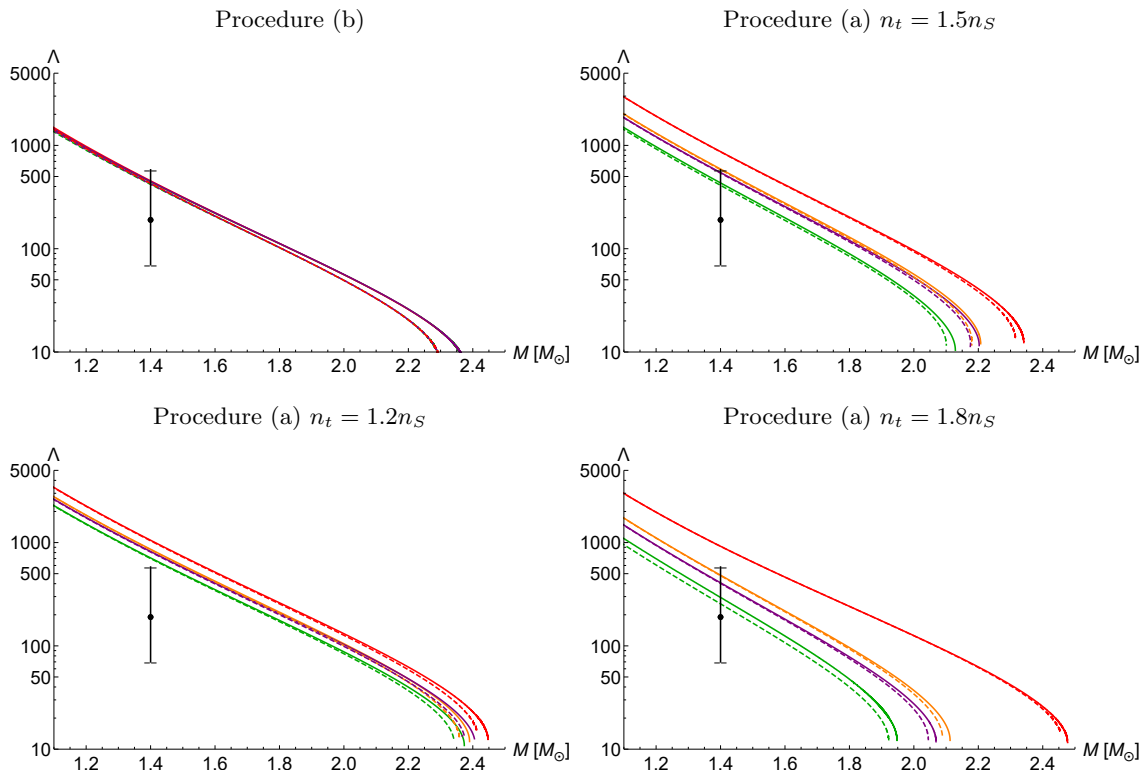


Figure 7. Mass-Tidal Deformability (MTD) curves for neutron stars. Top left panel: Matching procedure (b). Remaining panels: Matching procedure (a) with matching density n_t . For the color coding, see fig. 2.

Another property that we can compute having access to the EOS, is the tidal deformability Λ : It is defined from the tidal Love number k_2 and the star compactness $c = \frac{GM}{R}$ as

$$\Lambda = \frac{2k_2}{3c^2}. \quad (6.3)$$

In fig. 7 is shown the tidal deformability as function of the mass obtained for each EOS (MTD curves), together with the current most stringent bound from LIGO/Virgo GW1708-17 for a neutron star of mass $1.4M_\odot$. We see that models using the stiff variant of the HLPS EOS are in slight tension with the tidal deformability measurement.

Finally, in fig. 8 we display for illustrative purposes the density and composition of the entire neutron star as a function of its radius. In particular, the thick lines illustrate how large a fraction of the neutron star is made of the holographic QCD matter and

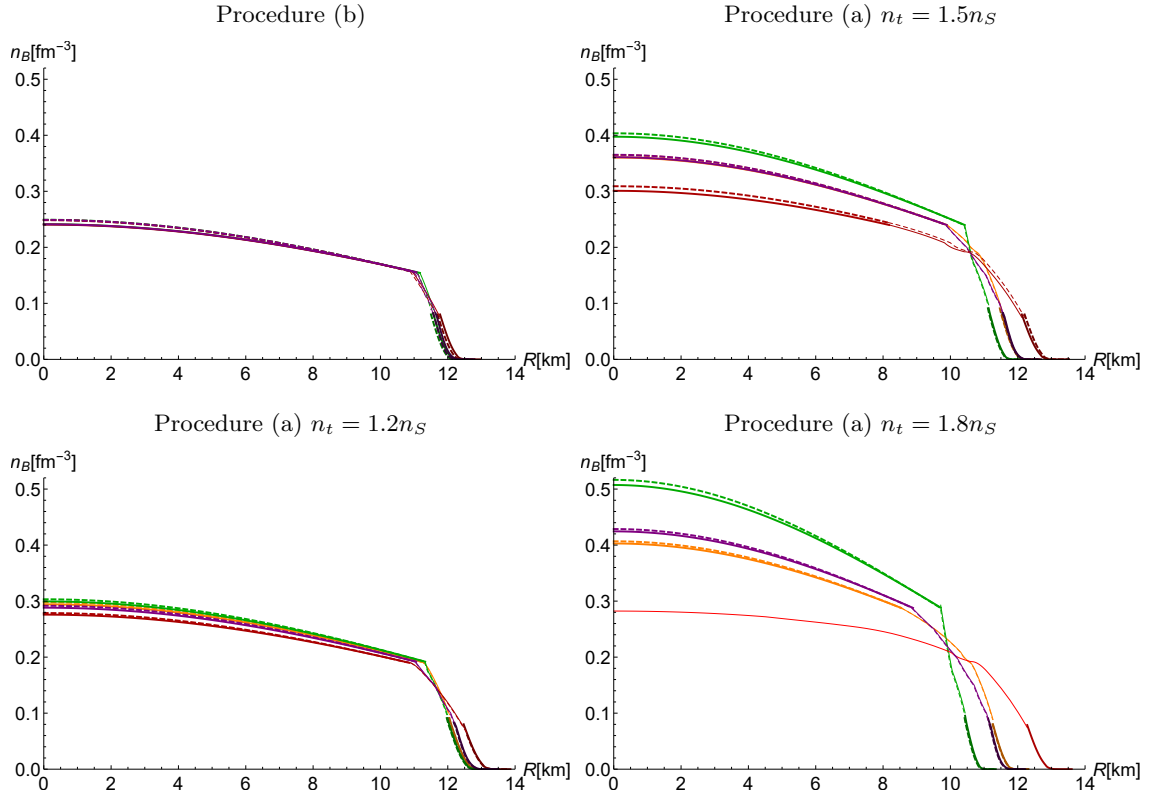


Figure 8. Density as a function of radial distance from the center of neutron stars, for typical stars of mass $1.4M_\odot$. Top left panel: Matching procedure (b). Remaining panels: Matching procedure (a) with matching density n_t . For the color coding, see fig. 2. Thick lines, thin lines, and darker thick lines correspond respectively to the holographic core, the low density core (HPLS or SLy4) and the crust of the stars. Note that in the bottom-right panel, only one red curve appears; this is because for this star the density never reaches the matching density $n_t = 0.288\text{fm}^{-3}$, and so it is insensitive to the holographic model.

what is made by the low-energy phenomenologically established equations of states. As an interesting example to point out, for the low matching density of $n_t = 1.2n_S$ (bottom-left panel) the holographic EOS is carrying most of the core of the star and does not change much with respect to the different low-energy EOSs (all about 11 to 11.5 km). On the other hand, for the high matching density $n_t = 1.8n_S$ (bottom-right panel), the holographic EOS simply does not enter the hybrid star that is soft in the low-density region (red thin line in the figure).

7 Conclusions

With this work, we have studied the effects of isospin breaking in nuclear matter within the holographic V-QCD model. A crucial simplifying approximation utilized in this work is the homogeneous Ansatz for nuclear matter, which consists of introducing a finite baryonic density via a discontinuity in the bulk gauge fields, which are taken to be independent of the position in three dimensional space. Isospin is introduced via an external chemical

potential, following the usual holographic prescription of encoding its value in the UV boundary condition for the field $A_t^{a=3}$. The approximation inherent in the homogeneous Ansatz is expected to be reliable only at high density: For this reason, we used a set of phenomenological equations of state for the description of the low-density regime (SLy4 and three representative HLPS). We considered two different approaches to matching the low density EOS with the holographic high density ones: The one labeled “procedure (a)” is more phenomenology-driven and corresponds to the introduction of a new parameter that acts as a rescaling factor for the holographic action, while with the one labeled “procedure (b)” avoid introducing new parameters and instead fit the already present ones to correctly reproduce the value of saturation density.

With this setup, expanding around the isospin symmetric configuration, we computed the symmetry energy of nuclear matter as a function of density, and compared its value around saturation density with phenomenology: We found remarkable agreement for procedure (a), while procedure (b) overestimates the symmetry energy at saturation, a result shared (though with milder magnitude) with other holographic models. Relaxing the assumption of small isospin, we solved the full system at arbitrary isospin and computed the EOS of β -equilibrated nuclear matter, complete with particle fractions (we have included massless electrons and massive muons to impose electric charge neutrality). For matching procedure (a) we have also included a transition to quark matter, while for procedure (b) it turned out to be impossible because of the mismatch in the scales of baryonic chemical potentials introduced by the choice of the single fit parameter b_1 : This problem is avoided in procedure (a) since the presence of two free parameters (b_1 and the rescaling c_b) allows for a matching of the scales of both densities and chemical potentials. We interpret the need for more free parameters as the compound error accumulated from two approximations: The restriction to the homogeneous Ansatz without other phases for holographic nuclear matter, and the use of the flat space expression for the tachyon potential in the Chern-Simons term. It would be interesting to explore how the results would change by considering different functional forms for the dilaton potential, a task we leave for the future.

Finally, having the computed EOS in hand, we solved the TOV equations and derived the properties of static neutron stars. We computed MR curves and tidal deformabilities of the stars resulting from each EOS, finding results that are in all cases close to observations, and a subset of EOSs that satisfy the constraints from NICER on the MR curves and from LIGO/Virgo on the tidal deformability. An interesting result is that those EOSs that produce neutron stars that satisfy these bounds are also those that correspond to parameters that correctly reproduced the phenomenological symmetry energy at saturation: This may hint that the rescaling procedure (a) tends to successfully capture some physics that is lost when taking the approximations of homogeneity and of the flat-space dilaton potential.

The introduction of isospin asymmetry is a direct improvement to the level of detail described within the already successful V-QCD model. There are, however, many other refinements that could be performed, but we would like to address two:

- Introduction of new phases: In this work we adopted only one configuration for

baryonic matter (and a similar one for quark matter), corresponding to the simplest case of a homogeneous distribution. It is not clear at what density this configuration becomes reliable, and it is expected that at lower density this approximation breaks down in favor of a spatially modulated configuration (possibly a lattice of baryons). While the inclusion of such phases may not be extremely relevant for procedure (a) since we transition to the holographic model only at higher densities, it may instead be crucial to obtain more realistic results within procedure (b) (or any other construction that employs the holographic model at lower densities). Moreover, a finite baryon number density may trigger an additional modulated instability driven by the TCS term [75–77], which may further complicate the phase diagram.

- Inclusion of the backreaction of baryons: In this work we considered the backreaction of quarks onto the geometry, but neglected it for the baryonic phase. While this approximation is reasonable, considering that the quark phase appears at much higher density than the baryonic one, it would be ideal to treat both phases on equal footings. A possible result of this improvement is a change in the position of the transition from baryonic to quark matter, that would have repercussions on the MR curves of neutron stars, in particular it could reduce the mass M_{TOV} of the heaviest stable stars.

These and other improvements are for now left for future works.

Acknowledgments

The work of L. B. is supported by the National Natural Science Foundation of China Youth Grant (Grant no. 12405084). S. B. G. thanks the Outstanding Talent Program of Henan University for partial support. M. J. has been supported by an appointment to the JRG Program at the APCTP through the Science and Technology Promotion Fund and Lottery Fund of the Korean Government and by the Korean Local Governments - Gyeongsangbuk-do Province and Pohang City - and by the National Research Foundation of Korea (NRF) funded by the Korean government (MSIT) (Grant no. 2021R1A2C1010834).

A Vanishing contribution of variation of r_c to the symmetry energy

In calculating the symmetry energy we assumed that the variation of the critical position, r_c , of the discontinuity in the bulk induced by the variation around isospin symmetry does not contribute to the result. Though intuitive, because of the perturbative argument, it is worthwhile showing explicitly that this is indeed the case. The symmetry energy is computed from the energy per baryon, which is in turn computed from the action: Introducing an infinitesimal isospin chemical potential, μ_I , we perturb the symmetric configuration, and then we read off the coefficient of the term quadratic in μ_I . We expand the Lagrangian density in unperturbed and quadratic terms:

$$\mathcal{L} = \mathcal{L}_0 + \mathcal{L}_2 \mu_I^2, \tag{A.1}$$

with \mathcal{L}_0 , \mathcal{L}_2 independent of μ_I . If the Lagrangian density vanishes for $r > r_c$, then the equilibrium condition reads:

$$\mathcal{L}_0(r_c) + \mathcal{L}_2(r_c)\mu_I^2 = 0. \quad (\text{A.2})$$

We can then expand also the critical radius r_c as:

$$r_c = r_{c0} + \delta r_c, \quad (\text{A.3})$$

with r_{c0} being the critical position of the discontinuity for symmetric matter, and δr_c being its μ_I -dependent infinitesimal variation. Imposing the equilibrium condition at the unperturbed order allows us to determine $\delta(r_c)$, which is also quadratic in μ_I :

$$\delta r_c = -\mathcal{L}_2(r_{c0})\mu_I^2 (\mathcal{L}'_0(r_{c0}))^{-1}. \quad (\text{A.4})$$

We now need to prove that the Lagrangian does not depend on δr_c at the quadratic order in μ_I . The Lagrangian is given by:

$$\begin{aligned} L &= \int_0^{r_c} dr (\mathcal{L}_0 + \mathcal{L}_2\mu_I^2) \\ &= \int_0^{r_{c0}} dr (\mathcal{L}_0 + \mathcal{L}_2\mu_I^2) + \int_{r_{c0}}^{r_{c0}+\delta r_c} dr (\mathcal{L}_0 + \mathcal{L}_2\mu_I^2) \\ &= \int_0^{r_{c0}} dr (\mathcal{L}_0 + \mathcal{L}_2\mu_I^2) + \delta r_c \mathcal{L}_0(r_{c0}) + \delta r_c \mathcal{L}_2(r_{c0})\mu_I^2. \end{aligned} \quad (\text{A.5})$$

The first term is the Lagrangian with the perturbation induced only at the field level, the one we use for the computation of the symmetry energy. The second term vanishes because $\mathcal{L}_0(r_{c0}) = 0$ by definition of r_{c0} . Finally, the third term only contributes at order μ_I^4 . \square

B Tables of parameters

In tab. 1 we report the choices of values of the parameters n_t, b_1, c_b for each hybrid equation of state. On the left are the choices for potentials 7a, while on the right for potentials 5b. In the last column labeled “Data” we evaluate the compatibility of the resulting neutron stars with the NICER and LIGO/Virgo data, indicating with a check mark \checkmark full compatibility, while with \times the presence of tension with the data currently available.

References

- [1] P. de Forcrand, *Simulating QCD at finite density*, *PoS LAT2009* (2009) 010, [[arXiv:1005.0539](#)].
- [2] J. M. Maldacena, *The Large N limit of superconformal field theories and supergravity*, *Adv. Theor. Math. Phys.* **2** (1998) 231–252, [[hep-th/9711200](#)].
- [3] H. Georgi, *Unparticle physics*, *Phys. Rev. Lett.* **98** (2007) 221601, [[hep-ph/0703260](#)].
- [4] A. Karch and E. Katz, *Adding flavor to AdS / CFT*, *JHEP* **06** (2002) 043, [[hep-th/0205236](#)].

V-QCD 7a	n_t	b_1	c_b	Data	V-QCD 5b	n_t	b_1	c_b	Data
HLPS soft	1.2	9.799	3.545	✗	HLPS soft	1.2	12.435	3.43	✗
HLPS int.	1.2	9.796	3.499	✗	HLPS int.	1.2	12.43	3.39	✗
HLPS stiff	1.2	9.867	3.287	✗	HLPS stiff	1.2	12.51	3.18	✗
SLy4	1.2	9.86	3.402	✗	SLy4	1.2	12.50	3.29	✗
HLPS soft	1.5	9.845	4.37	✓	HLPS soft	1.5	12.484	4.24	✓
HLPS int.	1.5	9.854	4.06	✓	HLPS int.	1.5	12.495	3.93	✓
HLPS stiff	1.5	9.93	3.55	✗	HLPS stiff	1.5	12.578	3.43	✗
SLy4	1.5	9.936	4.01	✓	SLy4	1.5	12.59	3.876	✓
HLPS soft	1.8	9.89	5.185	✗	HLPS soft	1.8	12.537	5.023	✗
HLPS int.	1.8	9.921	4.381	✓	HLPS int.	1.8	12.57	4.23	✓
HLPS stiff	1.8	9.696	3.269	✗	HLPS stiff	1.8	12.297	3.13	✗
SLy4	1.8	10.02	4.471	✓	SLy4	1.8	12.68	4.32	✓

Table 1. Summary of EOS and parameters for matching procedure (a).

- [5] E. Witten, *Anti-de Sitter space, thermal phase transition, and confinement in gauge theories*, *Adv. Theor. Math. Phys.* **2** (1998) 505–532, [[hep-th/9803131](#)].
- [6] T. Sakai and S. Sugimoto, *Low energy hadron physics in holographic QCD*, *Prog. Theor. Phys.* **113** (2005) 843–882, [[hep-th/0412141](#)].
- [7] J. Polchinski and M. J. Strassler, *Hard scattering and gauge / string duality*, *Phys. Rev. Lett.* **88** (2002) 031601, [[hep-th/0109174](#)].
- [8] A. Karch, E. Katz, D. T. Son, and M. A. Stephanov, *Linear confinement and AdS/QCD*, *Phys. Rev. D* **74** (2006) 015005, [[hep-ph/0602229](#)].
- [9] U. Gürsoy and E. Kiritsis, *Exploring improved holographic theories for QCD: Part I*, *JHEP* **02** (2008) 032, [[arXiv:0707.1324](#)].
- [10] U. Gürsoy, E. Kiritsis, and F. Nitti, *Exploring improved holographic theories for QCD: Part II*, *JHEP* **02** (2008) 019, [[arXiv:0707.1349](#)].
- [11] U. Gürsoy, E. Kiritsis, L. Mazzanti, and F. Nitti, *Holography and Thermodynamics of 5D Dilaton-gravity*, *JHEP* **05** (2009) 033, [[arXiv:0812.0792](#)].
- [12] U. Gürsoy, E. Kiritsis, L. Mazzanti, and F. Nitti, *Improved Holographic Yang-Mills at Finite Temperature: Comparison with Data*, *Nucl. Phys. B* **820** (2009) 148–177, [[arXiv:0903.2859](#)].
- [13] M. Järvinen and E. Kiritsis, *Holographic Models for QCD in the Veneziano Limit*, *JHEP* **03** (2012) 002, [[arXiv:1112.1261](#)].
- [14] M. Jarvinen, *Massive holographic QCD in the Veneziano limit*, *JHEP* **07** (2015) 033, [[arXiv:1501.07272](#)].

- [15] D. Arean, I. Iatrakis, M. Järvinen, and E. Kiritsis, *V-QCD: Spectra, the dilaton and the S-parameter*, *Phys. Lett. B* **720** (2013) 219–223, [[arXiv:1211.6125](#)].
- [16] D. Arean, I. Iatrakis, and M. Järvinen, *The spectrum of (h)QCD in the Veneziano limit*, *PoS Corfu2012* (2013) 129, [[arXiv:1305.6294](#)].
- [17] D. Areán, I. Iatrakis, M. Järvinen, and E. Kiritsis, *The discontinuities of conformal transitions and mass spectra of V-QCD*, *JHEP* **11** (2013) 068, [[arXiv:1309.2286](#)].
- [18] T. Alho, M. Järvinen, K. Kajantie, E. Kiritsis, and K. Tuominen, *On finite-temperature holographic QCD in the Veneziano limit*, *JHEP* **01** (2013) 093, [[arXiv:1210.4516](#)].
- [19] T. Alho, M. Järvinen, K. Kajantie, E. Kiritsis, C. Rosen, and K. Tuominen, *A holographic model for QCD in the Veneziano limit at finite temperature and density*, *JHEP* **04** (2014) 124, [[arXiv:1312.5199](#)]. [Erratum: *JHEP* **02**, 033 (2015)].
- [20] T. Alho, M. Jarvinen, K. Kajantie, E. Kiritsis, and K. Tuominen, *Quantum and stringy corrections to the equation of state of holographic QCD matter and the nature of the chiral transition*, *Phys. Rev. D* **91** (2015), no. 5 055017, [[arXiv:1501.06379](#)].
- [21] G. 't Hooft, *A Planar Diagram Theory for Strong Interactions*, *Nucl. Phys. B* **72** (1974) 461.
- [22] G. Veneziano, *Some Aspects of a Unified Approach to Gauge, Dual and Gribov Theories*, *Nucl. Phys. B* **117** (1976) 519–545.
- [23] M. Järvinen, *Holographic modeling of nuclear matter and neutron stars*, *Eur. Phys. J. C* **82** (2022), no. 4 282, [[arXiv:2110.08281](#)].
- [24] N. Kovensky, A. Poole, and A. Schmitt, *Building a realistic neutron star from holography*, *Phys. Rev. D* **105** (2022), no. 3 034022, [[arXiv:2111.03374](#)].
- [25] N. Kovensky, A. Poole, and A. Schmitt, *Predictions for neutron stars from holographic nuclear matter*, *SciPost Phys. Proc.* **6** (2022) 019, [[arXiv:2112.10633](#)].
- [26] L. Bartolini and S. B. Gudnason, *Neutron stars in the Witten-Sakai-Sugimoto model*, *JHEP* **11** (2023) 209, [[arXiv:2307.11886](#)].
- [27] C. Hoyos, D. Rodríguez Fernández, N. Jokela, and A. Vuorinen, *Holographic quark matter and neutron stars*, *Phys. Rev. Lett.* **117** (2016), no. 3 032501, [[arXiv:1603.02943](#)].
- [28] K. Bitaghsir Fadafan, J. Cruz Rojas, and N. Evans, *Deconfined, Massive Quark Phase at High Density and Compact Stars: A Holographic Study*, *Phys. Rev. D* **101** (2020), no. 12 126005, [[arXiv:1911.12705](#)].
- [29] K. Bitaghsir Fadafan, J. Cruz Rojas, and N. Evans, *Holographic quark matter with colour superconductivity and a stiff equation of state for compact stars*, *Phys. Rev. D* **103** (2021), no. 2 026012, [[arXiv:2009.14079](#)].
- [30] L. Bartolini, S. B. Gudnason, J. Leutgeb, and A. Rebhan, *Neutron stars and phase diagram in a hard-wall AdS/QCD model*, *Phys. Rev. D* **105** (2022), no. 12 126014, [[arXiv:2202.12845](#)].
- [31] N. Jokela, M. Järvinen, and J. Remes, *Holographic QCD in the Veneziano limit and neutron stars*, *JHEP* **03** (2019) 041, [[arXiv:1809.07770](#)].
- [32] P. M. Chesler, N. Jokela, A. Loeb, and A. Vuorinen, *Finite-temperature Equations of State for Neutron Star Mergers*, *Phys. Rev. D* **100** (2019), no. 6 066027, [[arXiv:1906.08440](#)].
- [33] C. Ecker, M. Järvinen, G. Nijs, and W. van der Schee, *Gravitational waves from holographic neutron star mergers*, *Phys. Rev. D* **101** (2020), no. 10 103006, [[arXiv:1908.03213](#)].

- [34] N. Jokela, M. Järvinen, G. Nijs, and J. Remes, *Unified weak and strong coupling framework for nuclear matter and neutron stars*, *Phys. Rev. D* **103** (2021), no. 8 086004, [[arXiv:2006.01141](#)].
- [35] M. Jarvinen, *Holographic baryons, dense matter and neutron star mergers*, *JHAP* **3** (2023), no. 3 1–22, [[arXiv:2307.01745](#)].
- [36] T. Demircik, C. Ecker, and M. Järvinen, *Dense and Hot QCD at Strong Coupling*, *Phys. Rev. X* **12** (2022), no. 4 041012, [[arXiv:2112.12157](#)].
- [37] S. Tootle, C. Ecker, K. Topolski, T. Demircik, M. Järvinen, and L. Rezzolla, *Quark formation and phenomenology in binary neutron-star mergers using V-QCD*, *SciPost Phys.* **13** (2022) 109, [[arXiv:2205.05691](#)].
- [38] C. Ecker, K. Topolski, M. Järvinen, and A. Stehr, *Prompt black hole formation in binary neutron star mergers*, *Phys. Rev. D* **111** (2025), no. 2 023001, [[arXiv:2402.11013](#)].
- [39] X.-Y. Liu, Y.-L. Wu, and Z. Fang, *A holographic study on QCD phase transition and neutron star properties*, [arXiv:2412.15149](#).
- [40] N. Kovensky and A. Schmitt, *Isospin asymmetry in holographic baryonic matter*, *SciPost Phys.* **11** (2021), no. 2 029, [[arXiv:2105.03218](#)].
- [41] L. Bartolini and S. B. Gudnason, *Symmetry energy in holographic QCD*, *SciPost Phys.* **16** (2024), no. 6 156, [[arXiv:2209.14309](#)].
- [42] N. Kovensky, A. Poole, and A. Schmitt, *Phases of cold holographic QCD: Baryons, pions and rho mesons*, *SciPost Phys.* **15** (2023), no. 4 162, [[arXiv:2302.10675](#)].
- [43] C. Adam, C. Naya, J. Sanchez-Guillen, R. Vazquez, and A. Wereszczynski, *BPS Skyrmions as neutron stars*, *Phys. Lett. B* **742** (2015) 136–142, [[arXiv:1407.3799](#)].
- [44] C. Adam, C. Naya, J. Sanchez-Guillen, R. Vazquez, and A. Wereszczynski, *Neutron stars in the Bogomol’nyi-Prasad-Sommerfield Skyrme model: Mean-field limit versus full field theory*, *Phys. Rev. C* **92** (2015), no. 2 025802, [[arXiv:1503.03095](#)].
- [45] C. Adam, J. Sanchez-Guillen, R. Vazquez, and A. Wereszczynski, *Adding crust to BPS Skyrme neutron stars*, *Phys. Rev. D* **102** (2020), no. 2 023019, [[arXiv:2004.03610](#)].
- [46] C. Adam, M. Huidobro, R. Vazquez, and A. Wereszczynski, *BPS Skyrme neutron stars in generalized gravity*, *JCAP* **08** (2020) 041, [[arXiv:2005.10834](#)].
- [47] C. Adam, A. Garcia Martin-Caro, M. Huidobro, R. Vázquez, and A. Wereszczynski, *A new consistent neutron star equation of state from a generalized Skyrme model*, *Phys. Lett. B* **811** (2020) 135928, [[arXiv:2006.07983](#)].
- [48] C. Adam, A. Garcia Martin-Caro, M. Huidobro, and A. Wereszczynski, *Skyrme Crystals, Nuclear Matter and Compact Stars*, *Symmetry* **15** (2023), no. 4 899, [[arXiv:2305.06639](#)].
- [49] P. Leask, M. Huidobro, and A. Wereszczynski, *Generalized skyrmion crystals with applications to neutron stars*, *Phys. Rev. D* **109** (2024), no. 5 056013, [[arXiv:2306.04533](#)].
- [50] S.-w. Li, A. Schmitt, and Q. Wang, *From holography towards real-world nuclear matter*, *Phys. Rev. D* **92** (2015), no. 2 026006, [[arXiv:1505.04886](#)].
- [51] V. Kaplunovsky and J. Sonnenschein, *Searching for an Attractive Force in Holographic Nuclear Physics*, *JHEP* **05** (2011) 058, [[arXiv:1003.2621](#)].
- [52] M. Jarvinen, V. Kaplunovsky, and J. Sonnenschein, *Many phases of generalized 3D instanton crystals*, *SciPost Phys.* **11** (2021), no. 1 018, [[arXiv:2011.05338](#)].

- [53] M. Järvinen, E. Kiritsis, F. Nitti, and E. Préau, *Tachyon-dependent Chern-Simons terms and the V-QCD baryon*, *JHEP* **12** (2022) 160, [[arXiv:2209.05868](#)].
- [54] M. Järvinen, E. Kiritsis, F. Nitti, and E. Préau, *The V-QCD baryon: numerical solution and baryon spectrum*, *JHEP* **05** (2023) 081, [[arXiv:2212.06747](#)].
- [55] R. Casero, E. Kiritsis, and A. Paredes, *Chiral symmetry breaking as open string tachyon condensation*, *Nucl. Phys. B* **787** (2007) 98–134, [[hep-th/0702155](#)].
- [56] F. Bigazzi, R. Casero, A. L. Cotrone, E. Kiritsis, and A. Paredes, *Non-critical holography and four-dimensional CFT's with fundamentals*, *JHEP* **10** (2005) 012, [[hep-th/0505140](#)].
- [57] T. Ishii, M. Järvinen, and G. Nijs, *Cool baryon and quark matter in holographic QCD*, *JHEP* **07** (2019) 003, [[arXiv:1903.06169](#)].
- [58] E. Witten, *Global Aspects of Current Algebra*, *Nucl. Phys. B* **223** (1983) 422–432.
- [59] O. Kaymakçalan, S. Rajeev, and J. Schechter, *Nonabelian Anomaly and Vector Meson Decays*, *Phys. Rev. D* **30** (1984) 594.
- [60] J. L. Manes, *Differential Geometric Construction of the Gauged Wess-Zumino Action*, *Nucl. Phys. B* **250** (1985) 369–384.
- [61] L. Bartolini and S. B. Gudnason, *Boundary terms in the Witten-Sakai-Sugimoto model at finite density*, *Phys. Rev. D* **109** (2024), no. 6 066006, [[arXiv:2309.16328](#)].
- [62] A. Amorim, M. S. Costa, and M. Järvinen, *Regge theory in a holographic dual of QCD in the Veneziano limit*, *JHEP* **07** (2021) 065, [[arXiv:2102.11296](#)].
- [63] K. Hebeler, J. M. Lattimer, C. J. Pethick, and A. Schwenk, *Equation of state and neutron star properties constrained by nuclear physics and observation*, *Astrophys. J.* **773** (2013) 11, [[arXiv:1303.4662](#)].
- [64] F. Douchin and P. Haensel, *A unified equation of state of dense matter and neutron star structure*, *Astron. Astrophys.* **380** (2001) 151, [[astro-ph/0111092](#)].
- [65] P. Haensel and B. Pichon, *Experimental nuclear masses and the ground state of cold dense matter*, *Astron. Astrophys.* **283** (1994) 313, [[nucl-th/9310003](#)].
- [66] M. Rozali, H.-H. Shieh, M. Van Raamsdonk, and J. Wu, *Cold Nuclear Matter In Holographic QCD*, *JHEP* **01** (2008) 053, [[arXiv:0708.1322](#)].
- [67] V. Kaplunovsky, D. Melnikov, and J. Sonnenschein, *Baryonic Popcorn*, *JHEP* **11** (2012) 047, [[arXiv:1201.1331](#)].
- [68] V. Kaplunovsky and J. Sonnenschein, *Dimension Changing Phase Transitions in Instanton Crystals*, *JHEP* **04** (2014) 022, [[arXiv:1304.7540](#)].
- [69] J. Cruz Rojas, T. Demircik, and M. Järvinen, *Popcorn Transitions and Approach to Conformality in Homogeneous Holographic Nuclear Matter*, *Symmetry* **15** (2023), no. 2 331, [[arXiv:2301.03173](#)].
- [70] T. E. Riley et al., *A NICER View of PSR J0030+0451: Millisecond Pulsar Parameter Estimation*, *Astrophys. J. Lett.* **887** (2019), no. 1 L21, [[arXiv:1912.05702](#)].
- [71] M. C. Miller et al., *PSR J0030+0451 Mass and Radius from NICER Data and Implications for the Properties of Neutron Star Matter*, *Astrophys. J. Lett.* **887** (2019), no. 1 L24, [[arXiv:1912.05705](#)].
- [72] T. E. Riley et al., *A NICER View of the Massive Pulsar PSR J0740+6620 Informed by Radio Timing and XMM-Newton Spectroscopy*, *Astrophys. J. Lett.* **918** (2021), no. 2 L27,

- [arXiv:2105.06980].
- [73] M. C. Miller et al., *The Radius of PSR J0740+6620 from NICER and XMM-Newton Data*, *Astrophys. J. Lett.* **918** (2021), no. 2 L28, [arXiv:2105.06979].
- [74] B. Margalit and B. D. Metzger, *Constraining the Maximum Mass of Neutron Stars From Multi-Messenger Observations of GW170817*, *Astrophys. J. Lett.* **850** (2017), no. 2 L19, [arXiv:1710.05938].
- [75] S. K. Domokos and J. A. Harvey, *Baryon number-induced Chern-Simons couplings of vector and axial-vector mesons in holographic QCD*, *Phys. Rev. Lett.* **99** (2007) 141602, [arXiv:0704.1604].
- [76] S. Nakamura, H. Ooguri, and C.-S. Park, *Gravity Dual of Spatially Modulated Phase*, *Phys. Rev. D* **81** (2010) 044018, [arXiv:0911.0679].
- [77] T. Demircik, N. Jokela, M. Jarvinen, and A. Piispa, *Is holographic quark-gluon plasma homogeneous?*, arXiv:2405.02392.